Stability near threshold in a semiconductor laser subject to optical feedback: A bifurcation analysis of the Lang-Kobayashi equations

Kirk Green
Department of Theoretical Physics, Vrije Universiteit, De Boelelaan 1081, 1081HV Amsterdam, The Netherlands
(Received 10 July 2008; revised manuscript received 10 October 2008; published 27 March 2009)

Through the use of analytical and numerical techniques, we investigate the interaction between the trivial off-state and the continuous-wave (CW) operation of a semiconductor laser subject to conventional optical feedback. More specifically, using numerical continuation tools, the stability and bifurcations of the CW states, or external-cavity modes (ECMs), are analyzed in dependence on the parameters of feedback phase, feedback strength, pump current, and the linewidth enhancement factor. In this way, curves of codimension-one Hopf bifurcations are shown to destabilize the off-state and lead to stable ECM operation. Moreover, self-intersections of these Hopf curves in codimension-two Hopf-Hopf bifurcation points are seen to give rise to curves of codimension-one torus bifurcations (Hopf bifurcations of the ECMs), and degenerate-Hopf points to the birth of saddle-node bifurcations of the ECMs, as parameters are varied. These codimension-two points are shown to come together at a codimension-three degenerate Hopf-Hopf point (a Bogdanov-Takens bifurcation of the ECMs): a limiting point for which a stable off-state can exist.

DOI: 10.1103/PhysRevE.79.036210 PACS number(s): 82.40.Bj, 42.55.Px, 42.65.Sf, 02.30.Oz

I. INTRODUCTION

In the past decade, great progress has been made in understanding the nonlinear dynamics of semiconductor lasers subject to external influences [1,2]. A large part of this understanding has been made possible through the use of numerical continuation software: tools which allow one to find and follow solutions of governing rate equations, irrespective of their stability. Moreover, by detecting and following changes in the stability of solutions, the *bifurcations*, continuation tools can be used to trace regions of different dynamical behavior in parameters. For example, a complete survey of the stability and bifurcations of the governing rate equations has been completed for semiconductor lasers subject to optical injection [3]. In particular, excellent theoretical agreement with experimental results has been achieved in terms of both the stability and of the bifurcations [4]: modeled by ordinary differential equations (ODEs), the bifurcations of the injection laser were mapped out using the continuation package AUTO [5]. A second form of external influence is that of *delayed optical feedback*, in which light leaving the laser is reflected back into it after a fixed time [6]. Uncontrolled optical feedback, for example, from an optical set-up component, may destabilize the continuous-wave (CW) operation of the laser [7]. However, controlled optical feedback has been shown to be beneficial in reducing the linewidth of the laser [8]; as a high-frequency optical signal generator [9]; and, more recently, as a chaotic signal generator for use in chaos communication schemes [10,11].

From a practical point of view, it is crucially important to understand the structure of the bifurcations which organize the different dynamical regimes of semiconductor lasers subject to external influences. In many applications that require CW output of the laser, such as for use in optical disk drives, laser spectroscopy or dentistry, the laser must operate in such a regime that any external influence, for example, back reflections from system components, do not destabilize the CW output or cause the laser to switch to coexisting CW states of different frequencies. In other words, knowledge of the closeness to instability, that is, to destabilizing bifurcations, of a desired CW state and the uniqueness of that particular solution is required. Conversely, one may want the laser to operate in a more complex nonlinear dynamical regime, such as for use in the aforementioned chaos communication schemes [10,11]. Here, one uses a controlled external influence to generate chaotic output of the laser light, which can then be used as a carrier wave on which to transmit confidential information; however, one must ensure that this chaotic regime is robust enough. That is to say, one must be operating in a parameter range so that small perturbations to the system do not cause a jump to a region of CW operation for which, if intercepted, the confidential information can be easily decrypted from the transmitted signal. A second nonlinear regime of interest may be that in which one finds a coexistence between a number of CW states. Such multistable operation could be exploited for use in, for example, optical flip-flop schemes [12]. For all of these areas of application, from the need for stable CW output, through to the want of a robust, more complex nonlinear dynamic, a detailed bifurcation analysis is of advantage in identifying the parameter ranges in which the laser must be operated in order to guarantee successful operation. Finally, from a design perspective, a detailed theoretical knowledge of the different dynamical regimes, and the bifurcations bounding these regimes, may be compared to experimental results in order to determine the values of hard to measure material properties of a given manufactured laser, such as the linewidth enhancement factor [13].

In the early 1980s, Lang and Kobayashi [14] proposed to model semiconductor lasers subject to conventional optical feedback (COF) using *delay differential equations* (DDEs). In order to solve DDEs, one must specify an initial history function: a "point" in an infinite-dimensional space of continuous functions [15]. The good news is that while DDEs have this infinite-dimensional phase space, their solutions have a discrete spectra and, therefore, the bifurcation theory

for ODEs can be applied [16,17]. It was not until relatively recently, however, that continuation tools for DDEs became available. The introduction of DDE-BIFTOOL [18] (a continuation package for the bifurcation analysis of DDEs) established a new era in the understanding of the bifurcations of semiconductor lasers subject to optical feedback. The COF laser was a driving force in the early development of DDE-BIFTOOL [19,20], however, the majority of bifurcation analyses of feedback lasers have been performed on Lang-Kobayashi-type rate equations describing more complicated feedback mechanisms, namely: phase-conjugate optical feedback (PCF) [21,22], filtered optical feedback (FOF) [23–26], mutually delay-coupled lasers [27,28], and both polarization resolved [29] and spatially extended [30] vertical-cavity surface-emitting lasers (VCSELs) subject to optical feedback; see also the survey [31]. Surprisingly, a full numerical bifurcation analysis of the COF laser (the system underlying the more complicated setups mentioned above) has escaped attention. Aside from the original analysis of Ref. [19], in which a partial two-parameter analysis in the planes of feedback phase versus both feedback strength and the linewidth enhancement factor were performed, continuation studies have been restricted to a single parameter [32–35]. Analytical two-parameter bifurcation analyses have proved to be more plentiful; see, for example, Refs. [36–40]. However, due to the infinite-dimensional nature of the governing DDE, a full stability analysis proved to be beyond the means of these analytical techniques.

It is the purpose of this paper to extend the results presented in the analytical studies [36–40], completing the numerical work of Ref. [19], where we will identify regions of stability of the so-called *external-cavity modes* (ECMs), the CW states, and the bifurcations bounding these regions in parameters. This paper constitutes a start toward a complete numerical survey of the stability and bifurcations of the COF laser, in parameters, akin to that which has been achieved for the injection laser [3]. Our study is organized as follows: in Sec. II the rate equations describing the COF laser are introduced; an analytical summary into the steady-state ECMs and the bifurcations they undergo is given in Sec. III; Sec. IV contains the results of our numerical bifurcation analysis where, in particular, we detail the interaction between the off-state of the COF laser and the ECMs as parameters are varied; and finally, in Sec. V we draw conclusions and discuss future work.

II. LANG-KOBAYASHI RATE EQUATIONS

In dimensionless form, the Lang-Kobayashi equations [14] describing the COF laser can be written as

$$\frac{dE}{dt} = (1 + i\alpha)EN + \kappa e^{-iC_p}E(t - \tau), \tag{1}$$

$$T\frac{dN}{dt} = P - N - (1 + 2N)|E|^2, \tag{2}$$

for the slowly varying complex electric field E and the inversion (number of electron-hole pairs) N. Parameters describe the linewidth enhancement factor α, the feedback strength κ, the 2π-periodic feedback phase C_p, the ratio between carrier and photon lifetimes T, and the pump current P. These equations are written in the frame of reference of the solitary laser threshold; that is, $P=0$ corresponds to the threshold pump current of the laser without feedback. Throughout this paper, we fix

$$\tau = 500 \text{ and } T = 1000. \tag{3}$$

These values were chosen so that our results can be compared to previous results obtained by numerical bifurcation analysis for the optical injection laser, PCF and FOF lasers, and mutually coupled lasers with delay. In particular, time is rescaled with respect to the photon lifetime $\tau_p = 1$ ps, so that a delay time of $\tau=500$ corresponds to an external cavity on the order of several centimeters.

III. ANALYTICAL SUMMARY

Before performing our numerical analysis, we briefly summarize some analytical results of Eqs. (1) and (2), where we follow the original line of thought of Ref. [41], together with insight that comes from the geometric bifurcation analysis techniques used in Refs. [42,40].

The trivial solution of Eqs. (1) and (2) is given as

$$(E,N) = (0,P). \tag{4}$$

We will refer to this zero-intensity solution as the *off-state* of the COF laser. As the level of feedback κ is increased from zero, additional solutions are known to emerge [14]. These solutions are called ECMs and are of the form

$$(E,N) = (R_s e^{i\omega_s t}, N_s). \tag{5}$$

In other words, they are solutions with a constant amplitude R_s, frequency ω_s, at a fixed level of inversion N_s; they are *continuous-wave* or CW states of the COF laser. Mathematically, the ECMs reflect the underlying S^1 symmetry of Eqs. (1) and (2) [43]; that is, they are invariant under the transformation

$$E \to cE \text{ where } \{c \in \mathbb{C}:\|c\| = 1\}. \tag{6}$$

It is well established [41] that substitution of Eq. (5) into Eqs. (1) and (2) yields the following sets of equations:

$$0 = N_s R_s + \kappa R_s \cos(C_p + \omega_s \tau + 2n\pi), \tag{7}$$

$$\omega_s = \alpha N_s - \kappa \sin(C_p + \omega_s \tau + 2n\pi), \tag{8}$$

$$0 = P - N_s - (1 + 2N_s)R_s^2, \tag{9}$$

where, throughout this paper, $n \in \mathbb{Z}$. These equations can be solved to give

$$\omega_s = -\frac{K}{\tau}\sin(\omega_s \tau + C_p + \arctan\ \alpha + 2n\pi), \tag{10}$$

$$N_s = -\kappa \cos(C_p + \omega_s \tau + 2n\pi), \tag{11}$$

$$R_s^2 = \frac{P - N_s}{1 + 2N_s}, \tag{12}$$

where the parameter

$$K = \kappa\tau\sqrt{1+\alpha^2} \tag{13}$$

describes the effective feedback strength [41]. We note already that $K<1$ is known as the *low feedback* regime and $K>1$ the *high feedback* regime. For $K<1$ only one ECM may exist, for $K>1$ more ECMs may exist [41].

Equation (10) is transcendental; that is, we cannot find ω_s explicitly. However, we can compute the values of ω_s numerically, which together with Eqs. (11) and (12) fully describe the ECMs. More specifically, one is interested in the roots of the nonlinear function

$$f(\omega_s) = \omega_s + \frac{K}{\tau}\sin(\omega_s\tau + C_p + \arctan\,\alpha + 2n\pi). \tag{14}$$

In the $[\omega_s, f(\omega_s)]$ plane, this describes a sinusoidally varying function along the diagonal $f(\omega_s)=\omega_s$. It is clear that the amplitude of this function is given by $K/\tau=\kappa\sqrt{1+\alpha^2}$, with frequency $1/\tau$; that is, as κ, α or τ are increased the number of solutions of Eq. (14) increases. Moreover, the feedback phase C_p shifts the sine curve along the diagonal. As it does so, ECMs are born in pairs when turning points of the curve pass through $f(\omega_s)=0$ [42,40]. Such a transition is indicative of a *saddle-node bifurcation of ECMs* (or double limit cycle bifurcation). They occur when

$$\frac{df(\omega_s)}{d\omega_s} = 0 \;\text{ and }\; f(\omega_s) = 0, \tag{15}$$

that is, saddle-node bifurcations (S^+ and S^-) of ECMs occur for

$$C_p = \pm\left\{\arccos\left(-\frac{1}{K}\right) + K\sin\left[\arccos\left(-\frac{1}{K}\right)\right]\right\} - \arctan\,\alpha + 2n\pi. \tag{16}$$

Clearly, they are independent of the pump current P. Note that this formula was first derived in Ref. [41] and is equivalent to that given in Ref. [40]. Furthermore, one can find the limiting parameter values for which these saddle-node bifurcations exist. Such points are identified as *cusp singularities*, they occur when

$$\frac{d^2f(\omega_s)}{d\omega_s^2} = 0 \;\text{ and }\; f(\omega_s) = 0, \tag{17}$$

that is, for

$$(C_p, \kappa) = \left(\pi - \arctan\,\alpha + 2n\pi, \frac{1}{\tau\sqrt{1+\alpha^2}}\right). \tag{18}$$

Note that this marks the transitional points between the low (one ECM) and high (many ECMs) feedback regimes; that is, the points at which $K=1$ [41,40].

Finally, we note one further bifurcation curve. By combining Eqs. (7) and (8), evaluated at $N_s=P$, one obtains

$$P^2 + (\alpha P - \omega_s)^2 = \kappa^2. \tag{19}$$

Again using Eq. (8), this can be written as

$$C_p = \pm\left[\arccos\left(-\frac{P}{\kappa}\right) + \tau\sqrt{\kappa^2 - P^2}\right] - \alpha\tau P + 2n\pi. \tag{20}$$

Equation (20) was derived from the assumption of an ECM with $N_s=P$ which implies $R_s=0$. In other words, along the curve given by Eq. (20) an ECM with zero intensity exists. [Apart from having a frequency component ω_s, this ECM is identical to off-state (4).] In Ref. [40], Eq. (20) is derived from a linear stability analysis of the off-state, where it was shown to be a curve of *Hopf bifurcations* which destabilize the off-state and lead to the birth of a single ECM.

The existence of ECMs [Eq. (14)], the saddle-node bifurcation [Eq. (16)], and the Hopf bifurcation of the off-state [Eq. (20)] complete our brief summary into the analytical bifurcation results which can be obtained by studying the geometry of the ECM solution curves. However, we are more interested in the interaction of these curves; the subtle changes in the bifurcation structure around threshold. Moreover, we want to analyze the destabilization of the ECMs in parameters. Asymptotic methods can be used to approximate the destabilizing Hopf bifurcations of ECMs [39]. Moreover, analytic expressions for the Hopf bifurcations of the full system [Eqs. (1) and (2)] (which are equivalent to torus bifurcations of the off-state [20]) can be obtained [40]. The problem is that, due to the infinite-dimensional nature of DDEs, they are always in the form of transcendental equations which need to be solved numerically. To this end, a numerical continuation tool such as AUTO could be used to solve these transcendental equations in parameters. However, it makes more sense to utilize the numerical continuation tool DDE-BIFTOOL [18] which allows one to find and follow solutions and bifurcations of the full DDE system, Eqs. (1) and (2), in parameters. As mentioned earlier, DDE-BIFTOOL has been used to great effect in studying semiconductor lasers subject to various forms of optical feedback [19,21–26,29,30].

IV. NUMERICAL BIFURCATION ANALYSIS

In order to perform a numerical bifurcation analysis of the ECMs of Eqs. (1) and (2) one must first resolve the underlying S^1 symmetry (6) [19,43]. This can be achieved by moving to a rotating frame of reference:

$$E \to Ee^{ibt}, \quad b \in \mathbb{R}. \tag{21}$$

The governing rate equations then become

$$\frac{dE}{dt} = (1 + i\alpha)EN + \kappa e^{-i(C_p + b\tau)}E(t-\tau) - ibE, \tag{22}$$

$$T\frac{dN}{dt} = P - N - (1 + 2N)|E|^2, \tag{23}$$

where $b \in \mathbb{R}$ is an additional unknown parameter. During numerical continuation, this is balanced through the inclusion

of the extra condition $\mathrm{Im}(E)=0$, thus a single solution is isolated. In this way, ECMs of the form (5) are now described as steady states of Eqs. (22) and (23), where the free parameter $b=-\omega_s$ at equilibrium [19].

A. Stability and bifurcations in the plane of feedback phase C_p versus pump current P

We begin our numerical analysis by considering the bifurcations of the off-state (4) and of the ECMs in the plane of feedback phase C_p versus pump current P, identifying changes in the bifurcation structure as the feedback strength κ is varied. All parameters are easily accessible in experiments [44,45]. Figure 1 shows a curve of Hopf bifurcations of the off-state h (black), curves of saddle-node bifurcations $S^{\pm}$ of the steady state ECMs (blue), and curves of Hopf bifurcations H of the ECMs (red) [17]. Interactions of these codimension-one bifurcations are marked by large dots (●); they include degenerate Hopf points $dh^{\pm}$, a codimension-two Hopf-Hopf point hh, and a codimension-three degenerate Hopf-Hopf point dhh. The bifurcation curves are drawn dark when supercritical, that is, the solution born in the bifurcation is stable, and light when subcritical, that is, the solution born in the bifurcation is unstable. Striped regions indicate areas in which the off-state (4) is stable, light green shading indicates regions in which a single ECM is stable, and dark green regions indicate bistability between ECMs. Note the 2π periodicity of the parameter C_p; that is, curves leaving the right boundary of each panel of Fig. 1 are continued at the left boundary. From Figs. 1(a)–1(c), the feedback strength κ is fixed at $\kappa=0.001$, 0.002, and 0.004, respectively.

Figure 1 clearly shows that as P is increased the stable off-state (striped region) is destabilized at the supercritical Hopf curve h (black), at which point a stable ECM is born (light green region). The curve h is given by Eq. (20) and is clearly seen to oscillate between $P=-\kappa$ and $P=\kappa$; compare with Eq. (19). Consequently, the lowest point for which a stable ECM exists can be derived from Eq. (20) as $(C_p,P)=(\alpha\kappa\tau+2n\pi,-\kappa)$. In other words, stable ECMs may exist below the solitary laser threshold $P=0$, the lower limit increasing with the feedback strength κ; this is known as *threshold reduction* [46]. Alternatively, for fixed values of P and as C_p is varied, it is seen that ECMs can also be born in supercritical saddle-node bifurcations $S^{\pm}$ (blue). In this case, two ECMs are born as a stable and unstable pair, often referred to as modes and antimodes [47]. Thus, one can find regions of bistability (dark green shading) between a stable ECM born at the curve h and a stable ECM born in a saddle-node bifurcation $S^{\pm}$. We note that while Eq. (14) is independent of P and, hence it follows, so is the saddle-node Eq. (16), solutions of form (5) can be complex; that is, they are not *physically relevant* [40]. For example, one finds no physically relevant ECMs in the purely striped region of Fig. 1, rather an ECM with a complex valued amplitude exists; as P is increased physically relevant ECMs are created only as the curve h is crossed. Hence, the saddle-node curves which give rise to *physically relevant* ECMs begin at the curves h at the points $dh^{\pm}$. At this point, the criticality of the curve h changes; this is characteristic of a *degenerate Hopf* point (also known as a generalized Hopf or Bautin bifurcation) [16,17]. Finally, it is seen in all cases that as P is increased, ECMs are destabilized in supercritical Hopf bifurcations H (red), leading to stable periodic oscillations of the output power $|E(t)|^2$ which upon variation in parameters may bifurcate into more complex, possibly chaotic, dynamics. These periodic solutions and their bifurcations can be analyzed using the continuation package PDDE-CONT [48], however, this is beyond the scope of this paper.

Having described the general features of Fig. 1, we now discuss the finer details of each panel. To help with our understanding, Fig. 2 shows one-parameter bifurcation diagrams cut through each panel of Fig. 1 at fixed values of P. These one-parameter bifurcation diagrams are also known as *ECM components*; we show them as a function of C_p against the constant level of inversion of the ECMs N_s (again, note the 2π periodicity of C_p). In Fig. 2, saddle-node bifurcations of ECMs are denoted by crosses (×), Hopf bifurcations of ECMs by stars (∗), and Hopf bifurcations of the off-state by large dots (●). Stable ECMs are drawn in green, unstable in red; the off-state (4) is drawn black when stable, gray when unstable. Note that the lower bound of each ECM component is given by $N_s=-\kappa$ and the upper bound by the smaller of $N_s=\kappa$ or $N_s=P$; compare with Eqs. (7) and (9). Furthermore, Fig. 3 shows the frequencies Ω_h and Ω_S of the ECMs born at the Hopf curve h (black) and the saddle-node curves $S^{\pm}$ (blue), respectively, together with the frequency Ω_H of the periodic modulation of the output power $|E(t)|^2$ arising at the Hopf curves H (red), as a function of the pump current P. From Figs. 3(a)–3(c), $\kappa=0.001$, 0.002, and 0.004, corresponding to the values of Figs. 1(a)–1(c). Note that these frequencies are independent of C_p.

Figure 2(a1) shows the ECM component for $(\kappa,P)=(0.001,-0.000\ 75)$. This is a transition just below the lower degenerate Hopf point dh^+ of Fig. 1(a). It is clear that a stable ECM is born from a supercritical Hopf bifurcation h of the stable off-state as C_p is both increased and decreased. Increasing P, one passes the point dh^+ in Fig. 1(a). Figure 2 (a2) for $(\kappa,P)=(0.001,0.000\ 25)$ shows the emergent saddle-node bifurcation on the rightmost turning point of the ECM component. The stable and unstable ECMs emanating from this point are both destroyed in Hopf bifurcations h as C_p is decreased. As the saddle-node bifurcation lies to the right of the Hopf bifurcation of the off-state, one finds a bistability between this off-state and an ECM. This is indicated in Fig. 1(a) by the light green, striped region between the curve S^+ and the curve h. Increasing P further, one passes the upper limit of the curve h. Consequently, the ECM component of Fig. 2 (a3) for $(\kappa,P)=(0.001,0.0015)$ does not terminate in a Hopf bifurcation of the off-state; the ECM component is now a smooth curve over all values of C_p. The second saddle-node bifurcation S^- is seen on the leftmost turning point of this ECM component. Moreover, for $P=0.0015$, the supercritical Hopf curve of ECMs H shown in Fig. 1(a) is crossed twice as C_p is decreased from $C_p=\pi$. Figure 2(a3) shows unstable ECMs (red) between these two Hopf bifurcations of ECMs. This leads to regions with no stable off-state or ECMs, the white regions of Fig. 1(a). Figure 3 also reveals the emergence of the Hopf curve H (red).

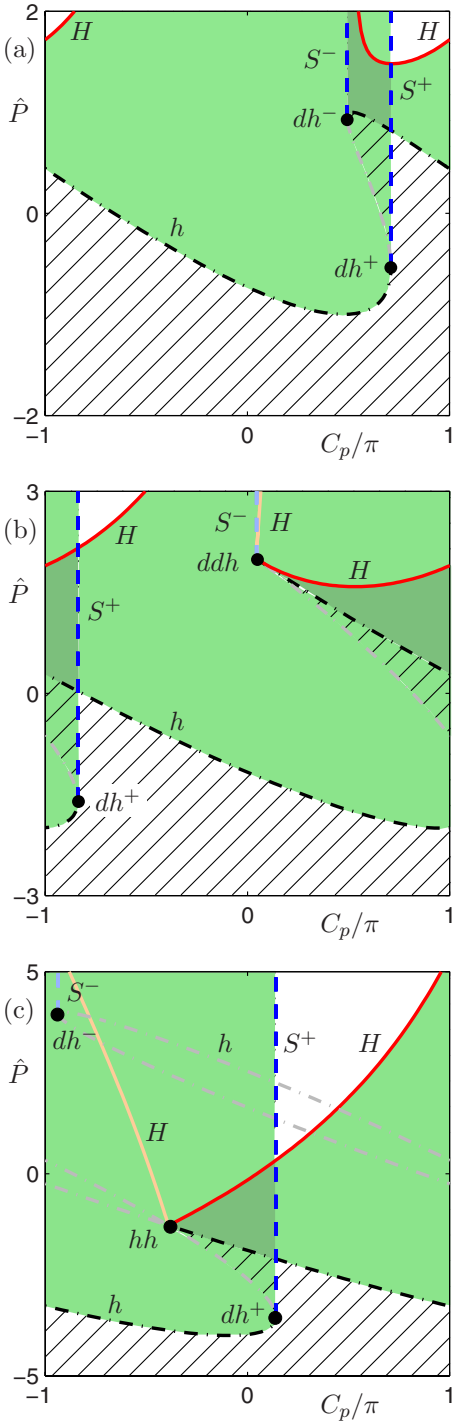

FIG. 1. (Color online) Two-parameter bifurcation diagrams of the off-state and the ECMs in the plane of feedback phase C_p versus pump current $\hat{P}=P\times 10^3$. From (a) to (c), the feedback strength $\kappa=0.001$, 0.002, and 0.004, respectively. Curves of Hopf bifurcations of the off-state h are drawn in black (dot-dashed curve), saddle-node bifurcations of ECMs $S^{\pm}$ in blue (dashed curve) and Hopf bifurcations of ECMS H in red (solid curve). Bifurcation curves are drawn dark when supercritical, light when subcritical. Striped regions indicate a stable off-state; light green shading, a stable ECM; darker shading, bistable ECMs; and regions of no shading indicate no stable off-state or ECM solution. Higher codimension degenerate Hopf points $dh^{\pm}$, a Hopf-Hopf bifurcation point hh, and a degenerate Hopf-Hopf point dhh, are indicated by large dots (●).

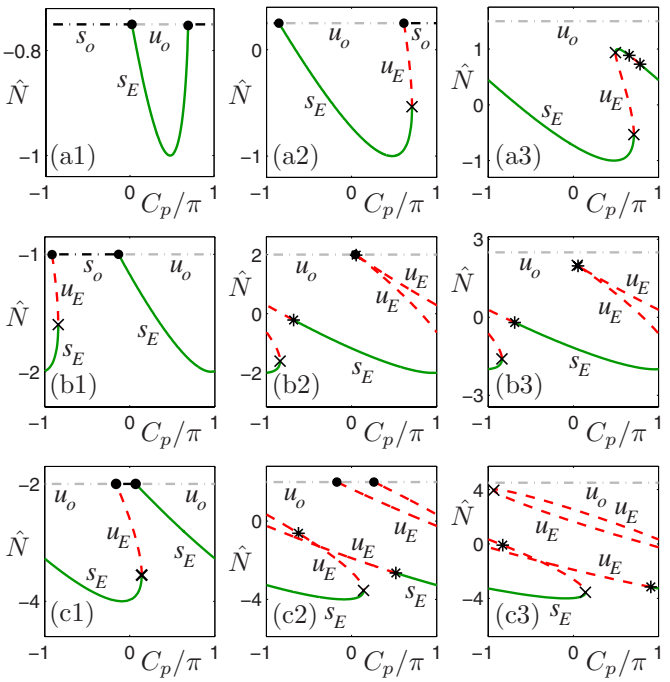

FIG. 2. (Color online) ECM components as a function of the feedback phase C_p. The vertical axis shows the steady-state value of inversion $\hat{N}=N_s\times 10^3$. Row (a) shows ECM components for feedback strength $\kappa=0.001$, where from (a1) to (a3), $P=-0.000\,75$, 0.00025, and 0.0015, respectively; row (b) for $\kappa=0.002$, where from (b1) to (b3), $P=-0.001$, 0.002, and 0.0025, respectively; and row (c) for $\kappa=0.004$, where from (c1) to (c3), $P=-0.002$, 0.002, and 0.0045, respectively. Stable ECMs s_E are drawn in green (solid curve), unstable u_E in red (dashed curve); stable off-states s_o are drawn in black, unstable u_o in gray (dot-dashed curves). Saddle-node bifurcations of ECMs are marked by a cross (×), Hopf bifurcations of ECMs by a star (*), and Hopf bifurcations of the off-state by a large dot (●).

At this low value of $\kappa=0.001$, the frequency Ω_H of the bifurcating periodic modulation is approximately that of the *undamped relaxation oscillations* (ROs); namely, $\Omega_H\approx\Omega_{\mathrm{RO}}=\sqrt{2P/T}=0.002|_{P=0.002}$.

The bifurcation scenario becomes more complicated as κ is increased. Locally, the key transition occurs at $\kappa=1/\tau=0.002$; this is shown in Fig. 1(b). The curve h is seen to form a geometric *cusp*. The curve S^- and the curve H identified in Fig. 1(a) are shown to emanate from this cusp point.

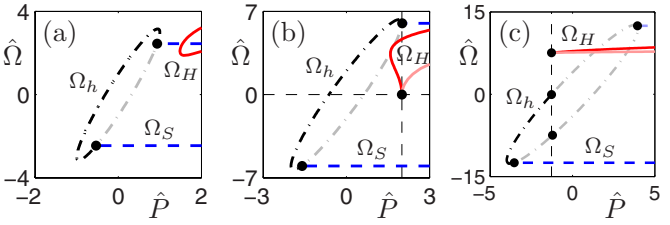

FIG. 3. (Color online) Frequencies $\hat{\Omega}=\Omega\times 10^3$ of the Hopf bifurcation of the off-state Ω_h (black dot-dashed curve), the ECMs at the saddle-node bifurcations Ω_S (blue dashed curves), and the Hopf bifurcations Ω_H (red solid curves), along the bifurcation curves shown in Fig. 1.

In fact, the curve H now consists of two separate parts, a supercritical part (dark red), leading to loss of stability of an ECM and the birth of a stable periodic solution, and a subcritical part (light red), leading to no changes in ECM stability and the birth of an unstable periodic solution. This is typical of a Hopf-Hopf point hh [16,17]. Moreover, the curve S^- is obviously that which was shown to emerge from the degenerate Hopf point dh^- in Fig. 1(a). Therefore, we will refer to this codimension-three point, at the cusp of the curve h and from which the curves S^- and H emanate, as the *degenerate Hopf-Hopf* point dhh. It occurs at $(C_p,\kappa,P)=(\pi-\alpha+2n\pi,1/\tau,1/\tau)=(0.1416+2n\pi,0.002,0.002)$. Again, we aid our description of Fig. 1(b) with ECM components. These are shown in Figs. 2(b1) to 2(b3) for $P=-0.001$, 0.002, and 0.0025, respectively. Once more, for low values of P, but above the point dh^+ one finds bistability between the off-state and an ECM; see Fig. 2(b1) and the green, striped region of Fig. 1(b). At the degenerate value of $(\kappa,P)=(0.002,0.002)$, Fig. 2(b2) shows that the ECM component forms a cusp, the tip of which is the codimension-three point dhh. Past this value of P, the subcritical saddle-node bifurcation S^- exists and the off-state is always unstable; see Fig. 2(b3) and compare with Fig. 1(b). Again, the frequencies Ω of the respective bifurcating solutions are shown in Fig. 3(b). The curve S^- is clearly seen to emanate from the rightmost turning point of the curve h, the point of Hopf degeneracy. At this point, the lower and upper parts of the curve h come together, at the same frequency: the point dhh. Moreover, the frequencies Ω_H, of the bifurcating modulation, along the curve H are seen to go to zero for $P=0.002$. This can be interpreted as a Bogdanov-Takens bifurcation BT of the ECMs (or, indeed, a 1:1 resonance of the off-state, at which point the ECM bifurcating from the curve h has leading multipliers $\mu_{1,2}=1$). Physically, the low frequency solutions emanating from the curve H, near the point dhh, are a source of excitability [49]: one finds nearby infinite-period homoclinic solutions [17].

Finally, for values of $\kappa>1/\tau=0.002$, Fig. 1(c) shows that after the cusp, the curve h has a self-intersection. Again, supercritical and subcritical curves H are still seen to emanate from this codimension-two Hopf-Hopf bifurcation point hh [16,17]; compare with Ref. [20]. Note that such a bifurcation has also been identified in the *inversionless laser* [50]. Figure 3(c) reveals that the frequencies Ω_h of the ECMs emanating from the supercritical and subcritical parts of the curve h are now different at the point hh. Moreover, the frequency Ω_H of the bifurcating periodic modulation at the curve H is seen to be well above $\Omega_{\mathrm{RO}}\approx 0.0032|_{P=0.005}$. In fact, Ω_H is seen to be approximately the difference between the two frequencies Ω_h; we will return to this later at the end of Sec. IV B. The associated ECM components at $\kappa=0.004$ are shown in Figs. 2(c1) to 2(c3) for $P=-0.002$, 0.002, and 0.0045, respectively. For these higher values of κ, the ECM component may terminate in subcritical Hopf bifurcations of the off-state at both ends; see Fig. 2 (c2) for $P=0.002$. Figure 2 (c3) also reveals that, as C_p is varied, the ECM component may pass through more than one 2π interval before terminating. This is to be expected, as we have already noted that increasing κ, or indeed P, leads to an increase in the number of coexisting, physically relevant ECMs.

We end our discussion on the stability and bifurcations of the ECMs in the (C_p,P)-parameter plane by briefly investigating what happens at higher values of the pump current P (although this is away from threshold, the bifurcation structure remains simple and, hence, it is worth the brief excursion). Figures 4(a)–4(c) again show regions of ECM stability and their bifurcations for $\kappa=0.001$, 0.002, and 0.004, respectively, but extended into higher values of P. In general, as P is increased curves of Hopf bifurcations of ECMs (red) are seen to appear. For $\kappa=0.001$, Fig. 4(a), these Hopf curves are shown to be closed. The lowest curve is a continuation of the curve H identified in Fig. 1(a). As κ is increased, these closed Hopf curves may overlap; see Fig. 4(b) for $\kappa=0.002$. Intersections between the top and bottom of two neighboring Hopf curves occur at codimension-two Hopf-Hopf bifurcation points HH (marked as large dots in Fig. 4). From such points curves of torus bifurcations of ECMs emanate (these are equivalent to bifurcations of the off-state to T^3 tori [47]), giving rise to quasiperiodic modulations in the output power $|E(t)|^2$, which in turn may bifurcate to more complicated, chaotic dynamics [7]. Furthermore, the Hopf curves form tangencies with the saddle-node curve S^- at codimension-two saddle-node Hopf bifurcation points SH^- (indicated by the large dots which lie on the vertical saddle-node curve S^-). Again, curves of torus bifurcations are known to emanate from such points [16,17]. The situation gets more complicated as κ is increased; see Fig. 4(c) for $\kappa=0.004$. The number of Hopf curves at higher values of P increases. Moreover, one observes regions of tristability between ECMs marked by the darkest green region in Fig. 4(c).

B. Stability and bifurcations in the plane of feedback phase C_p versus feedback strength κ

We now investigate the stability and bifurcations of the ECMs in the plane of feedback phase C_p versus feedback strength κ, for different values of the pump current P. This projection was used in Ref. [19] and the analytical studies of Refs. [38,40]. Figures 5(a)–5(f) show two-parameter bifurcation diagrams for $P=-0.001$, 0.0, 0.0005, 0.001, 0.002, and 0.005, respectively. Bifurcations and regions of stability of the off-state and the ECMs are color coded as in Figs. 1 and 4. Figure 5(a) for $P=-0.001$ shows that for values of pump current below threshold, the off-state is stable at the onset of feedback. For most values of C_p, as κ is increased the off-state is destabilized at the supercritical curve h (black), at which point a single stable ECM is born (recall threshold reduction [46]). The exception to this is found for $C_p\in[-3.497+2n\pi,-1.135+2n\pi]$. In this range of C_p, Fig. 5(a) shows that a stable ECM is born (together with an unstable ECM) at the curve S^+ (blue). (This curve S^+ begins at the degenerate Hopf point dh^+.) Thus, like for Fig. 1, one observes a region of bistability between the off-state and an ECM (light green, striped region). This region of bistability is bounded above by the curve h in which the off-state is destabilized. Furthermore, for $C_p\in[-1.642+2n\pi,1.772+2n\pi]$ the ECM born at the curve h coexists with the stable ECM born in the saddle-node bifurcation S^+; one finds a region of bistable ECMs (shaded dark green). As for Fig. 1,

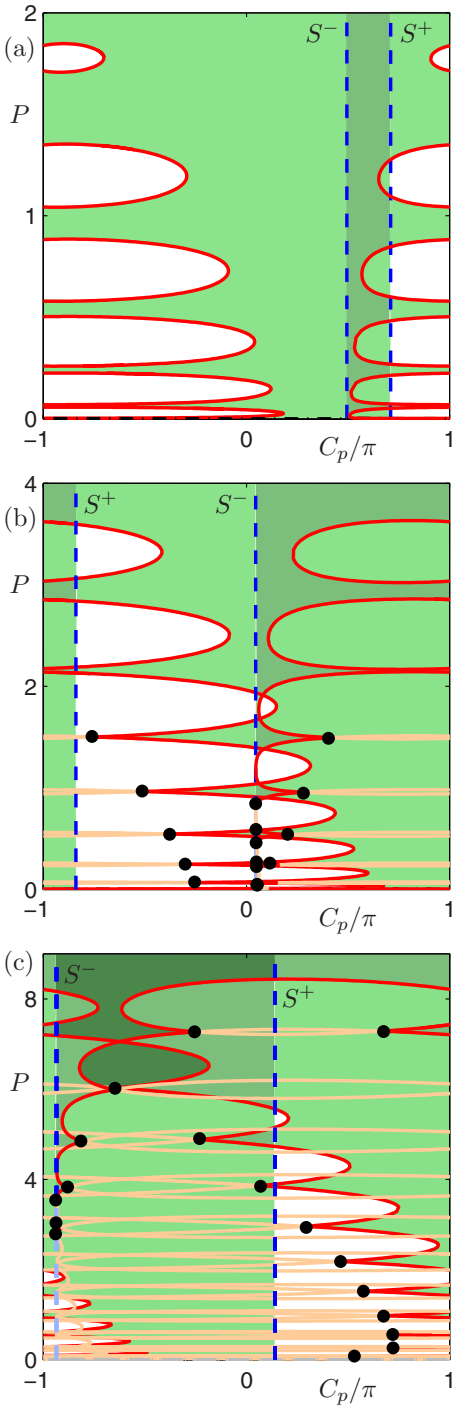

FIG. 4. (Color online) Extension of Fig. 1 into higher values of the pump current $P(=\hat{P}\times 10^{-3})$. Shaded as for Fig. 1 with the addition of a darker region in panel (c) indicating regions of tristable ECMs. The large dots (●) mark the intersection of two Hopf curves (red solid curves) at codimension-two Hopf-Hopf points *hh*, and the intersection of Hopf and saddle-node curves S^- (blue dashed curves) at saddle-node Hopf points SH^-.

the criticality of the curve *h* changes when it intersects itself. Again, from this codimension-two Hopf-Hopf point *hh*, two curves *H* are seen to emanate. As κ is increased, ECMs are destabilized at the supercritical one of these (dark red). This can lead to regions containing no stable off-state or ECMs (white). Finally, at higher values of κ, stable ECMs are born in the continuation of the curve S^+. This generic scenario of ECMs born in supercritical saddle-node bifurcations and being destabilized in supercritical Hopf bifurcations occurs for all values of pump current *P*; see already Figs. 5(b)–5(f). The crucial changes between each panel of Fig. 5 involve the interaction of the curves $S^\pm$ and *h*, around the degenerate Hopf points $dh^\pm$.

Figure 5(b) shows the case for $P=0$; that is, at the threshold value of the solitary laser. This is clearly a degenerate situation. The curves *h* are symmetric about $C_p=0$ and form straight lines from $\kappa=0$, extending into higher values. From Eq. (20), these curves *h* are given as $C_p=\pm(\pi/2+\kappa\tau)+2n\pi$. The points *hh* are found at $C_p=n\pi$. Again, one observes a region of bistability between the off-state and an ECM (light green, striped region), and a region of bistability between two ECMs (shaded dark green).

For values of pump current above threshold, Fig. 5(c) for $P=0.0005$ shows that a stable ECM is born at the onset of feedback $\kappa=0$ for all values of C_p. This is a consequence of the curve *h* folding over on itself to form a small loop; the bifurcation from a stable off-state to a stable ECM occurs as one moves from the inside of this loop to the outside. The off-state is only stable inside this small loop. Furthermore, the curve S^- which begins at the point dh^- is seen to pass through this loop. (Note that the point dh^+ has now changed to dh^- as a cusp in the saddle-node curve has formed.) Thus, one still finds a small region of bistability between the stable off-state and an ECM. As the pump current *P* is increased, the *h* loop can be seen to tighten. This results in the destruction of the region in which one finds a stable off-state only; see Fig. 5(d) for $P=0.001$. The loop in the curve *h* tightens to a point for $P=1/\tau=0.002$; see Fig. 5(e). The resulting cusp is that identified in Fig. 1(b) and occurs at the codimension-three point *dhh*. The curve *h* which emanates from this point *dhh* is now subcritical along its entire length; for $P\geq 1/\tau=0.002$ a stable off-state can no longer exist. Moreover, the supercritical curves *H* are seen to contort to lower values of κ. This results in the loss of the large regions of ECM bistability (dark green). Finally, Fig. 1(f) for $P=0.005$ shows that as the pump current *P* is increased, the point dh^- has moved along a diagonal toward lower values of C_p (modulus 2π). In doing so, it drags a subcritical part of the saddle-node curve S^- (light blue) with it. The change in criticality of this curve S^- happens at a codimension-two saddle-node Hopf bifurcation point SH^-, a remnant of the unfolding of the codimension-three point *dhh*. This is the scenario one finds for higher values of *P*, and that identified in Ref. [19]. Specifically, one finds diagonal bands of ECM stability bounded below by curves of supercritical saddle-node bifurcations and above by curves of supercritical Hopf bifurcations, the latter emanating from a codimension-two point SH^-.

We now return to considering the frequencies of the bifurcating solutions, this time as a function of κ. Figures 6(a)–6(c) show these frequencies, color coded as in Fig. 3, for $P=0.001$, 0.002, and 0.005; that is, corresponding to the bifurcation diagrams of Figs. 5(d)–5(f), respectively. It is clear that for higher values of κ the frequency Ω_H of the curves *H* asymptote to similar values. In fact, for $\kappa>1/\tau$

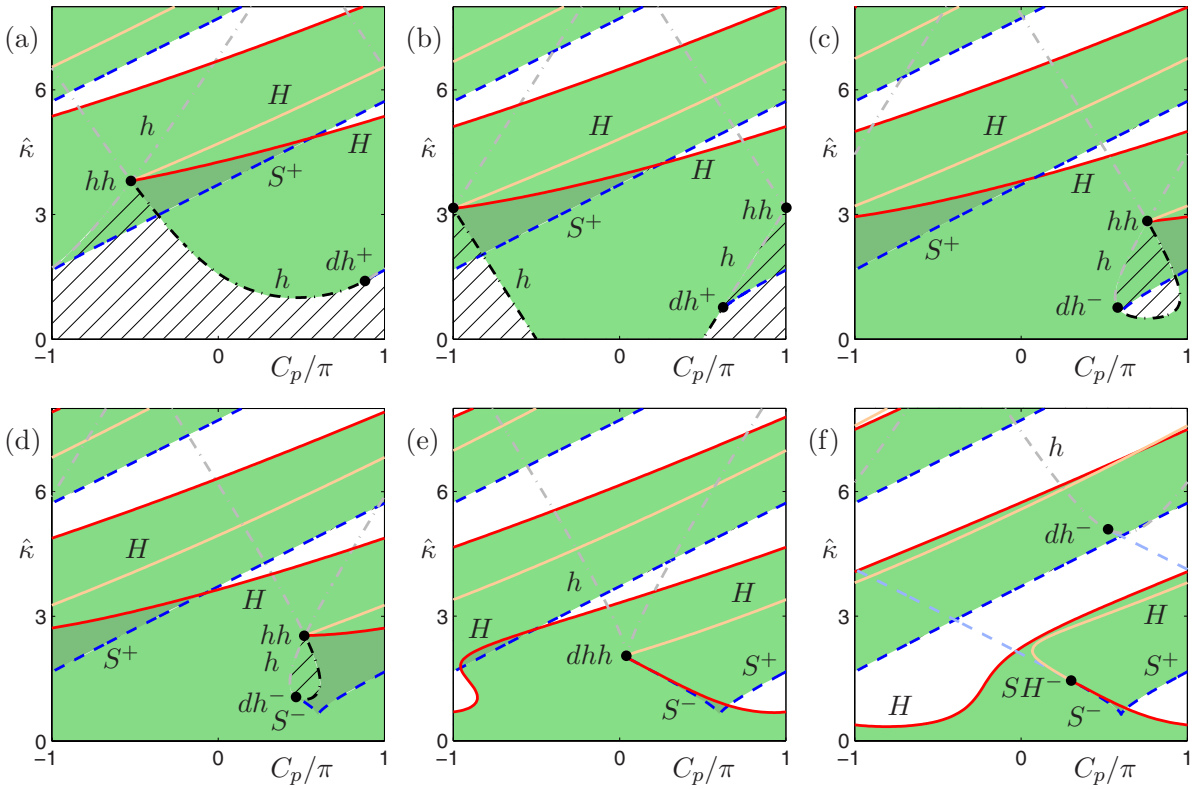

FIG. 5. (Color online) Two-parameter bifurcation diagrams of the off-state and the ECMs in the plane of feedback phase C_p versus feedback strength $\hat{\kappa}=\kappa\times 10^3$. From (a) to (f), the pump current $P=-0.001$, 0.0, 0.0005, 0.001, 0.002, and 0.005, respectively. Curves of Hopf bifurcations of the off-state h are drawn in black (dot-dashed curve), saddle-node bifurcations of ECMs $S^{\pm}$ in blue (dashed curve) and Hopf bifurcations of ECMs H in red (solid curve). Bifurcation curves are drawn dark when supercritical, light when subcritical. Striped regions indicate a stable off-state; light green shading, a stable ECM; darker shading, bistable ECMs; and regions of no shading indicate no stable steady state solution. Higher codimension degenerate Hopf points $dh^{\pm}$, Hopf-Hopf bifurcation points hh, saddle-node Hopf bifurcations SH and a degenerate Hopf-Hopf point dhh, are indicated by large dots (●).

$=0.002$ the supercritical part of this curve is known to follow an asymptotic approximation identified by Tager and Petermann (TP) along which one finds two ECMs at identical levels of inversion, yet with differing frequencies [39,51,52]. The oscillation born along this supercritical part of the Hopf curve (for $\kappa>1/\tau=0.002$) has been shown to exhibit a frequency given by the difference of the two ECM frequencies

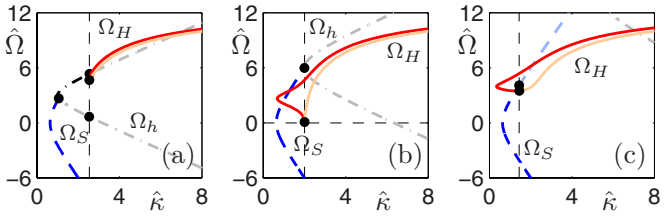

FIG. 6. (Color online) Frequencies $\hat{\Omega}=\Omega\times 10^3$ of the Hopf bifurcation of the off-state Ω_h (black dot-dashed curve), and of the ECMs at the saddle-node bifurcations Ω_S (blue dashed curve) and the Hopf bifurcations Ω_H (red solid curves), as a function of the feedback strength $\hat{\kappa}=\kappa\times 10^3$ for $P=0.001$ (a), 0.002 (b), and 0.005 (c). The large dots correspond to codimension-two points: a degenerate Hopf point dh and a Hopf-Hopf point hh, in (a); a degenerate Hopf-Hopf point dhh, in (b); and a saddle-node Hopf point SH^{-}, in (c); compare with Figs. 5(d)–5(f).

[32,51]; this was identified in Fig. 3(c). Figure 6 also agrees with the observation of Ref. [52] that the frequency of the oscillations have an upper bound of $\Omega=2\pi/\tau\approx 0.012$. For $\kappa<1/\tau=0.002$, Figs. 6(b) and 6(c) show a slight kink in the upper part of the supercritical Hopf curve, where it starts to follow a second asymptotic approximation [52]. For very short external cavities, the oscillations emanating from the Hopf curve following this second asymptote have been termed dispersive self Q-switching (DQS) pulsations [53]. As noted above, they are characterized by frequencies on the time-scale of undamped relaxation oscillations $\Omega_{\mathrm{RO}}=\sqrt{2P/T}$; that is, around $\Omega=0.002$ in Fig. 6(b) and around $\Omega=0.0032$ in Fig. 6(c). The PT and DQS asymptotes are known to converge at a single point of mode degeneracy (MD) at which the two ECM frequencies responsible for these pulsations are equal. Close to this MD point one finds the saddle-node Hopf points identified in Figs. 5(f) and 6(c) [52,53]. Further to this, as for Fig. 3(b), Fig. 6(b) reveals that for the degenerate case of $P=1/\tau=0.002$, the frequency of the Hopf curves decreases below Ω_{RO} to a value of $\Omega=0$ at $\kappa=1/\tau=0.002$, the codimension-three point dhh. As noted, the oscillations emanating from the Hopf curves close to the point dhh (identified in Fig. 5(e)) have extremely low frequencies (or large periods) indicating the presence of nearby homoclinic dynamics [17,49,53].

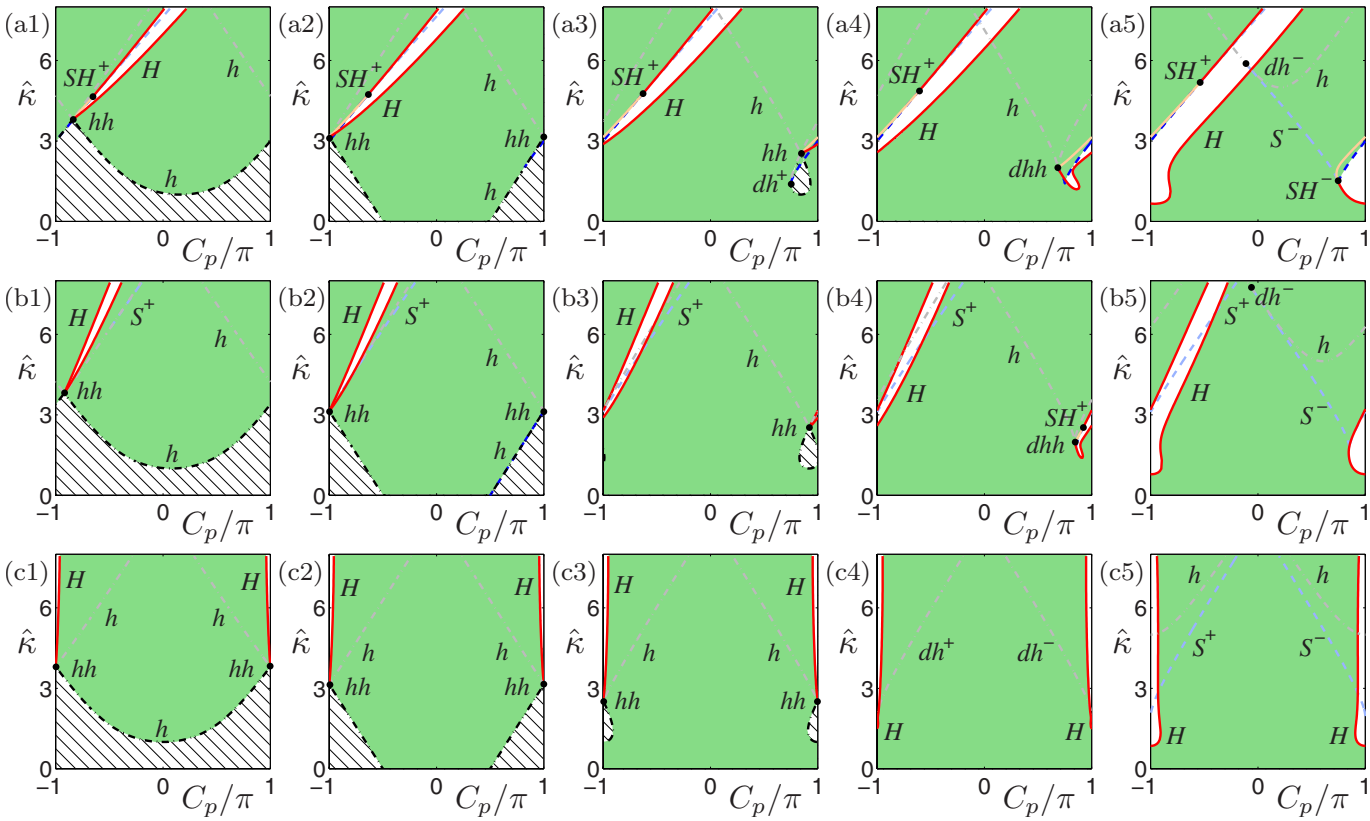

FIG. 7. (Color online) Extension of Fig. 5 into lower values of the linewidth enhancement factor α. From row (a) to row (c), $\alpha=1$, 0.5 and 0, respectively; from column 1 to column 5, $P=-0.001$, 0.0, 0.001, 0.002 and 0.005, respectively (see the caption of Fig. 1 for shading detail).

C. Changes in the linewidth enhancement factor α

We end our study by considering what effect a decrease in the linewidth enhancement factor α has on the bifurcation structure. Figure 7 shows bifurcation diagrams for $\alpha=1.0$, 0.5 and 0.0 [rows (a) to (c), respectively], and for $P=-0.001$, 0.0, 0.001, 0.002, and 0.005 [columns 1–5, respectively], in the plane of feedback phase C_p versus feedback strength κ. Physically, Eqs. (1) and (2) at these low values of α are used to model microchip lasers [54]. Figure 7 [rows (a) and (b)] show that, for $\alpha=1$ and 0.5, the bifurcation structure is qualitatively the same as for $\alpha=3$ (Fig. 5). Moreover, as α is decreased [Figs. 7(a)–7(c)], the h curves simply shift with respect to C_p: for $P<0$, this curve moves to lower values of C_p; for $P=0$, the curve does not move; and for $P>0$, it moves to higher values of C_p [this can be inferred from Eq. (20)]. The main difference with Fig. 5 is the emergence of an SH^+ point on the upper H curve. This point moves down the H curve as α is decreased. In doing so, the H curve changes to supercritical and the S^+ curve turns subcritical. Eventually, the SH^+ point reaches the point hh and disappears, the two H curves emanating from the point hh are then both seen to be supercritical. A second change, as α is decreased, is that the curves H move toward the vertical: the regions of ECM instability become smaller and, above threshold, our whole region of interest is dominated by a single stable ECM. The feedback sensitivity is very much reduced for lower values of α [55]. This is leading toward the degenerate situation of zero linewidth enhancement factor.

Figure 7 [row (c)], for $\alpha=0$, shows that the bifurcation structure is symmetric about $C_p=2n\pi$; compare Eq. (8) with $(C_p,\omega_s)\to(-C_p,-\omega_s)$. The only stable ECM is born at the supercritical curve h (below threshold) or at the onset of feedback $\kappa=0$. Moreover, this ECM is shown to be unstable only in thin regions bounded by the H curves around $C_p=(2n+1)\pi$. This instability is due to the negative interference between the outgoing and the reflected electric field. No ECMs are born in saddle-node bifurcations: all of the curves $S^\pm$ are subcritical. In fact, one only finds curves $S^\pm$ in Fig. 7 (c5) for $P=0.005$. As P is decreased, the curve h moves closer to the curves $S^\pm$ until, for $P=1/\tau=0.002$ [Fig. 7 (c4)], the curves lie on top of one another: the degenerate Hopf interaction takes place along the entire curve. For $\alpha=0$, in fact, this degeneracy only exists at $P=1/\tau$; compare Ref. [40] (the equation for "κ^*"). For $P<0.002$, the curves $S^\pm$ no longer exist.

Finally, Fig. 8 shows bifurcation diagrams in the (C_p,α) plane. This is for completeness and should be compared to the early study of Ref. [36]. From rows (a) to (c), $\kappa=0.001$, 0.002, and 0.003. As for Fig. 7, from column 1 to column 5, $P=-0.001$, 0.0, 0.001, 0.002, and 0.005, respectively. The symmetry between positive and negative values of α is immediately clear; that is under the transformation $(C_p,\alpha)\to-(C_p,\alpha)$. Furthermore, for fixed κ and P, the curves h are seen to be linear with slope $-1/(P\tau)$; recall Eq. (20). For values of $\kappa\leq|P|$ where $P<0$, Fig. 8(a1) shows that the off-state is the only stable solution for all values of C_p and α;

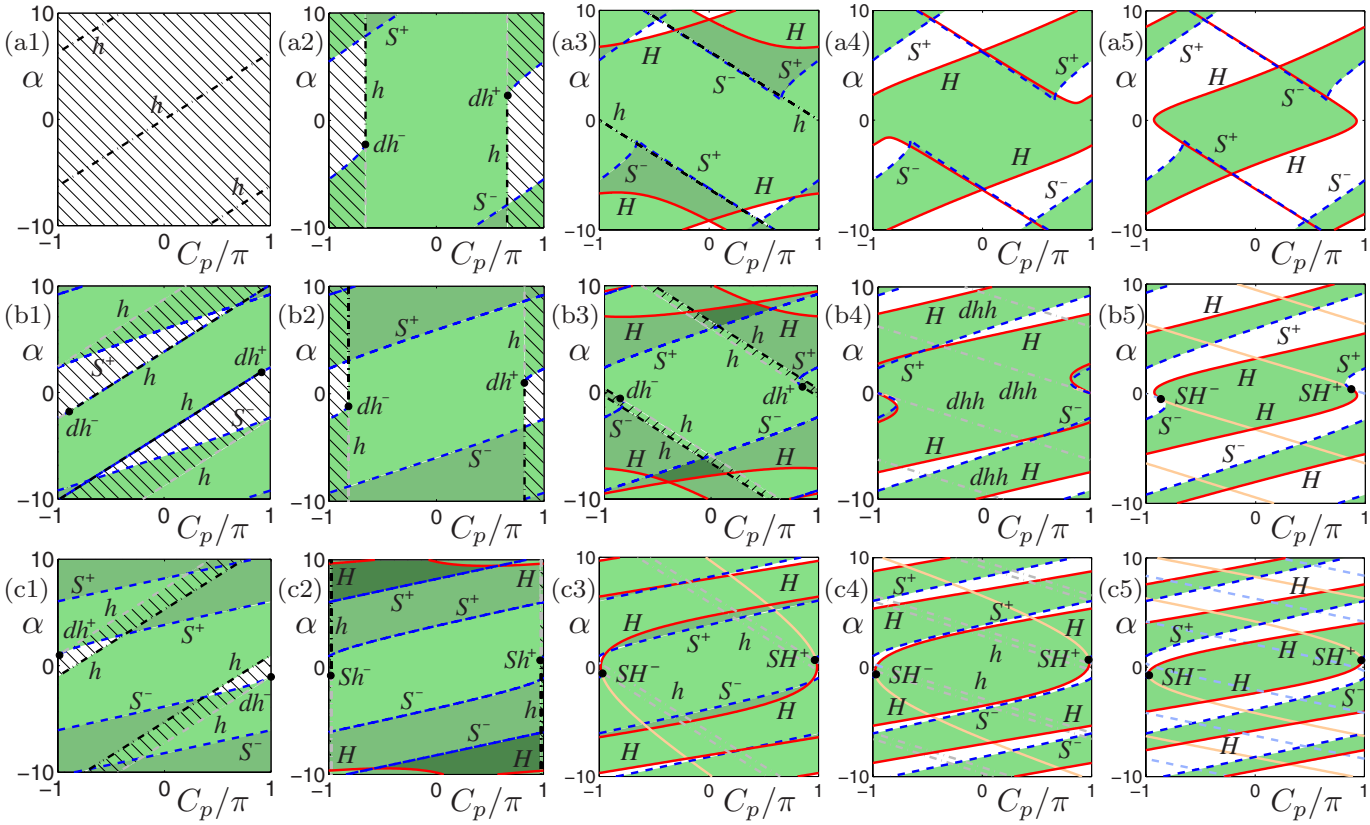

FIG. 8. (Color online) Two-parameter bifurcation diagrams of the off-state and the ECMs in the plane of feedback phase C_p versus the linewidth enhancement factor α. From row (a) to row (c), κ=0.001, 0.002, and 0.003, respectively; from column 1 to column 5, P=−0.001, 0.0, 0.001, 0.002 and 0.005, respectively (see the caption of Fig. 1 for shading detail).

compare with Figs. 5(a) and 7 (column 1). The curves h in Fig. 8(a1) are double covered. Figure 8(b1) shows that as κ is increased, they move apart to reveal a region of single ECM stability. Moreover, curves $S^{\pm}$ enter our region of interest [compare with Fig. 5(a)] resulting in regions of bistability between the off-state and the ECM, or indeed between the ECM and a second stable ECM born at these curves $S^{\pm}$. Increasing κ results in further multistability where one observes regions of tristability between the off-state and the two ECMs; see Fig. 8(c1). The situation is more complex for higher values of P. At threshold, P=0, Fig. 8(b1) again reveals regions of bistability. As κ is increased [Fig. 8(b2)], yet more curves $S^{\pm}$ enter our region of interest, resulting in additional stable ECMs and, subsequently, in regions of tristability between three stable ECMs for large values of α; see Fig. 8(c2). Moreover, the supercritical curves h move increasingly closer together leading to smaller regions of stability of the off-state. One also observes the emergence of the curves H in Fig. 8(c2). For values of P above threshold, these curves H are more prominent. Figure 8(a3) for (κ, P) =(0.001,0.001) shows that they lead to regions of no stable off-state or ECMs. However, the double covered curves h open as κ is increased to reveal a small region of bistability between the off-state and a stable ECM; see Fig. 8 (b3): one is moving upwards through the loop in the curve h shown in Fig. 7 column 3. Also from Fig. 8(a3)–8(b3), the degree of multistability is again seen to increase through the emergence of $S^{\pm}$ curves, however, it decreases in Fig. 8(c3) due to the dominance of the destabilizing curves H. As P is increased, Fig. 8 columns 4 and 5 show increasing sizes to the regions in which one finds no stable off-state or ECMs. The principal difference being that for higher values of κ [rows (b)-(c)], further $S^{\pm}$ and H curves enter our region of interest so that the regions of no stability are interspersed by regions in which one finds a single stable ECM. Figure 8 column 5 can be qualitatively compared to the bifurcation diagrams of Ref. [36]. Finally, we draw attention to the degenerate case $\kappa = P = 1/\tau = 0.002$, shown in Fig. 8(b4), in which one finds a curve of degenerate Hopf-Hopf bifurcations of the off-state *dhh*.

V. CONCLUSIONS

We have performed a thorough numerical bifurcation analysis of the steady states of a semiconductor laser subject to conventional optical feedback (COF), as modeled by the Lang-Kobayashi equations. Specifically, we have investigated what effect changes in the values of the experimentally accessible parameters of pump current P, feedback strength κ and feedback phase C_p have on the stability of the laser's off-state and of the continuous-wave, external-cavity modes (ECMs). Moreover, we also investigated the effect of varying the linewidth enhancement factor α. Such studies, assuming a knowledge of κ and P, can be used to determine the α factor experimentally [13]. Furthermore, our study allows comparison with similar bifurcation results obtained from the

analysis of semiconductor lasers subject to filtered optical feedback, mutually coupled lasers with delay and spatially extended lasers subject to optical feedback; all modeled by increasingly complicated extensions to the Lang-Kobayashi equations. In this way, our study is a foundation against which to compare these more complicated models and future studies.

While it has been well documented that as the feedback strength is increased, the ECMs of the COF laser are born in saddle-node bifurcations and destabilized in Hopf bifurcations, and to a lesser extent that these bifurcations are organized around codimension-two bifurcation points, we have shown how these organizing centers interact under the variation of further parameters. As our study progressed, the bifurcation diagrams became increasingly more complicated. However, it is hoped that by explaining the initial results in detail, the latter results are clear. Multistability between the off-state and the ECMs was found to increase for larger values of the linewidth enhancement factor. Moreover, the bifurcation structure was seen to be organized by codimension-two degenerate Hopf and Hopf-Hopf bifurcation points of the off-state. The codimension-three point at which these two Hopf degeneracies came together was shown to be the limit for which a stable off-state can exist.

Challenges still remain for this most fundamental of all semiconductor feedback laser systems. As already mentioned, the periodic solutions of the ECMs (those which emanate from the supercritical Hopf bifurcations), and their bifurcations, can be mapped out in parameters [48], thus, identifying regions of chaotic output and adding robustness to chaotic communication schemes [10]. Furthermore, homoclinic bifurcations of the periodic solutions are known to guide the well-documented low frequency fluctuations (LFF) [33,56]. A detailed examination of these homoclinic bifurcations, in parameters, may locate the organizing center of the LFF. Finally, it is hoped that a detailed study, akin to that of Ref. [4], in which the bifurcations of the COF laser are mapped out experimentally may reproduce the numerical bifurcation curves presented here.

[1] *Fundamental Issues of Nonlinear Laser Dynamics*, edited by B. Krauskopf and D. Lenstra, AIP Conf. Proc. No. 548 (AIP, New York, 2000).

[2] G. H. M. van Tartwijk and D. Lenstra, Quantum Semiclassic. Opt. **7**, 87 (1995).

[3] S. Wieczorek, B. Krauskopf, T. B. Simpson, and D. Lenstra, Phys. Rep. **416**, 1 (2005).

[4] S. Wieczorek, T. B. Simpson, B. Krauskopf, and D. Lenstra, Phys. Rev. E **65**, 045207(R) (2002).

[5] E. Doedel, A. R. Champneys, T. Fairgrieve, Yu. Kuznetsov, B. Sandstede, and X. Wang, AUTO 97: Continuation and bifurcation software for ordinary differential equations, 1997 (Available from http://indy.cs.concordia.ca/auto/main.html).

[6] K. Petermann, IEEE J. Sel. Top. Quantum Electron. **1**, 480 (1995).

[7] D. Lenstra, B. H. Verbeek, and A. J. den Boef, IEEE J. Quantum Electron. **21**, 674 (1985).

[8] M. W. Fleming and A. Mooradian, IEEE J. Quantum Electron. **17**, 44 (1981).

[9] T.-C. Yen, J.-W. Chang, J.-M. Lin, and R.-J. Chen, Opt. Commun. **150**, 158 (1998).

[10] G. D. VanWiggeren and R. Roy, Science **279**, 1198 (1998).

[11] G. D. Van Wiggeren and R. Roy, Phys. Rev. Lett. **88**, 097903 (2002).

[12] C.-H. Lee, K.-H. Cho, S.-Y. Shin, and S.-O. Lee, IEEE J. Quantum Electron. **24**, 2063 (1988).

[13] Y. Yu, G. Giuliani, and S. Donati, IEEE Photon. Technol. Lett. **16**, 990 (2004).

[14] R. Lang and K. Kobayashi, IEEE J. Quantum Electron. **16**, 347 (1980).

[15] J. K. Hale and S. M. Verduyn Lunel, *Introduction to Functional Differential Equations* (Springer-Verlag, Berlin, 1993).

[16] J. Guckenheimer and P. Holmes, *Nonlinear Oscillations, Dynamical Systems, and Bifurcations of Vector Fields* (Springer-Verlag, New York, 1983).

[17] Yu. Kuznetsov, *Elements of Applied Bifurcation Theory* (Springer, Berlin, 1995).

[18] K. Engelborghs, T. Luzyanina, G. Samaey, D. Roose, and K. Verheyden, DDE-BIFTOOL V. 2.03: A MATLAB package for bifurcation analysis of delay differential equations, 2001 (Available from http://ftp.cs.kuleuven.ac.be/twr/research/software/delay/ddebiftool.shtml).

[19] B. Haegeman, K. Engelborghs, D. Roose, D. Pieroux, and T. Erneux, Phys. Rev. E **66**, 046216 (2002).

[20] D. Pieroux, T. Erneux, T. Luzyanina, and K. Engelborghs, Phys. Rev. E **63**, 036211 (2001).

[21] K. Green, B. Krauskopf, and G. Samaey, SIAM J. Appl. Dyn. Syst. **2**, 254 (2003).

[22] K. Green and B. Krauskopf, Opt. Commun. **231**, 383 (2004).

[23] H. Erzgräber, B. Krauskopf, D. Lenstra, A. P. A. Fischer, and G. Vemuri, Phys. Rev. E **73**, 055201(R) (2006).

[24] H. Erzgräber, D. Lenstra, B. Krauskopf, A. P. A. Fischer, and G. Vemuri, Phys. Rev. E **76**, 026212 (2007).

[25] H. Erzgräber, B. Krauskopf, and D. Lenstra, SIAM J. Appl. Dyn. Syst. **6**, 1 (2007).

[26] H. Erzgräber and B. Krauskopf, Opt. Lett. **32**, 2441 (2007).

[27] H. Erzgräber, D. Lenstra, B. Krauskopf, E. Wille, M. Peil, I. Fischer, and W. Elsäßer, Opt. Commun. **255**, 286 (2005).

[28] H. Erzgräber, B. Krauskopf, and D. Lenstra, SIAM J. Appl. Dyn. Syst. **5**, 30 (2006).

[29] M. Sciamanna, T. Erneux, F. Rogister, O. Deparis, P. Mégret, and M. Blondel, Phys. Rev. A **65**, 041801(R) (2002).

[30] K. Green, B. Krauskopf, and D. Lenstra, Opt. Commun. **277**, 359 (2007).

[31] B. Krauskopf, in *Bifurcation Analysis of Lasers with Delay*, edited by D. M. Kane and K. A. Shore, Unlocking Dynamical Diversity: Optical Feedback Effects on Semiconductor Lasers (Wiley, New York, 2005), p. 147.

[32] D. Pieroux, T. Erneux, B. Haegeman, K. Engelborghs, and D. Roose, Phys. Rev. Lett. **87**, 193901 (2001).

[33] D. Pieroux and P. Mandel, Phys. Rev. E **68**, 036204 (2003).
[34] M. Sciamanna, P. Mégret, and M. Blondel, Phys. Rev. E **69**, 046209 (2004).
[35] A. Tabaka, K. Panajotov, I. Veretennicoff, and M. Sciamanna, Phys. Rev. E **70**, 036211 (2004).
[36] B. Tromborg, J. H. Osmundsen, and H. Olesen, IEEE J. Quantum Electron. **20**, 1023 (1984).
[37] A. Ritter and H. Haug, J. Opt. Soc. Am. B **10**, 130 (1993).
[38] A. M. Levine, G. H. M. van Tartwijk, D. Lenstra, and T. Erneux, Phys. Rev. A **52**, R3436 (1995).
[39] T. Erneux, Proc. SPIE **3944**, 588 (2000).
[40] V. Rottschäfer and B. Krauskopf, Int. J. Bifurcat. Chaos **17**, 1575 (2007).
[41] G. A. Acket, D. Lenstra, A. J. den Boef, and B. H. Verbeek, IEEE J. Quantum Electron. **20**, 1163 (1984).
[42] K. Green and B. Krauskopf, Opt. Commun. **258**, 243 (2006).
[43] B. Krauskopf, G. H. M. van Tartwijk, and G. R. Gray, Opt. Commun. **177**, 347 (2000).
[44] T. Heil, I. Fischer, W. Elsäßer, B. Krauskopf, K. Green, and A. Gavrielides, Phys. Rev. E **67**, 066214 (2003).
[45] J. Mork, J. Mark, and B. Tromborg, Phys. Rev. Lett. **65**, 1999 (1990).
[46] A. Olsson and C. L. Tang, IEEE J. Quantum Electron. **17**, 1320 (1981).
[47] J. Mørk, J. Mark, and B. Tromborg, IEEE J. Quantum Electron. **28**, 93 (1992).
[48] R. Szalai, PDDE-CONT: A continuation and bifurcation software for delay-differential equations, 2005. (Available from http://seis.bris.ac.uk/rs1909/pdde/).
[49] B. Krauskopf, K. Schneider, J. Sieber, S. Wieczorek, and M. Wolfrum, Opt. Commun. **215**, 367 (2002).
[50] S. Wieczorek and W. W. Chow, Phys. Rev. Lett. **97**, 113903 (2006).
[51] A. A. Tager and K. Petermann, IEEE J. Quantum Electron. **30**, 1553 (1994).
[52] M. Wolfrum and D. Turaev, Opt. Commun. **212**, 127 (2002).
[53] J. Sieber, SIAM J. Appl. Dyn. Syst. **1**, 248 (2002).
[54] E. Lacot and O. Hugon, Appl. Opt. **43**, 4915 (2004).
[55] N. Schunk and K. Pertermann, IEEE J. Quantum Electron. **24**, 1242 (1988).
[56] T. Sano, Phys. Rev. A **50**, 2719 (1994).